AMERICAN SOCIETY FOR MICROBIOLOGY | Antimicrobial Agents and Chemotherapy

In vivo pharmacodynamic characterization of a next-generation polyene, SF001, in the invasive pulmonary aspergillosis mouse model

Alexander J. Lepak,[1] Brian VanScoy,[2] Chris Rubino,[2] Paul G. Ambrose,[2] David R. Andes[1,3,4]

AUTHOR AFFILIATIONS See affiliation list on p. 12.

ABSTRACT SF001 is a next-generation polyene antifungal drug in development, designed to have increased specificity to fungal ergosterol, which is absent in humans, and decreased binding to cholesterol. SF001 demonstrates long-acting, potent, broad-spectrum fungicidal activity. The goal of the current study was to determine the pharmacodynamic index and target of SF001 in an immunocompromised mouse model of invasive pulmonary aspergillosis against six *Aspergillus fumigatus* isolates. Minimum inhibitory concentration (MIC) values ranged from 0.5 to 2.0 mg/L. Plasma and epithelial lining fluid (ELF) pharmacokinetics were performed following single intraperitoneal doses of 1, 4, 16, and 64 mg/kg. Treatment efficacy was assessed with each of the six fungal isolates using daily doses of SF001 ranging from 0.25 to 64 mg/kg/day over a 96-h treatment duration. Efficacy was assessed by *A. fumigatus* quantitative PCR of conidial equivalents from lung homogenates. Nonlinear regression analysis using the Hill equation demonstrated that the 24-h exposure-response relationships for both plasma and ELF area under the concentration/MIC and C_{max}/MIC ratios were strong and relatively similar [coefficient of determination (R^2) = 0.74–0.75). Exposure-response relationships included a median plasma 24-h C_{max}/MIC target for stasis and 1-log kill endpoint of 0.5 and 0.6, respectively. The present studies demonstrated *in vitro* and *in vivo* SF001 potency against *A. fumigatus*. These results have potential relevance for SF001 clinical dose selection and evaluation of susceptibility breakpoints.

KEYWORDS SF001, amphotericin, pharmacodynamics, *Aspergillus*

Invasive pulmonary aspergillosis (IPA), most frequently caused by *Aspergillus fumigatus*, is a leading cause of mortality in immunocompromised patients, in particular those with solid organ and bone marrow transplantation (1, 2). Additionally, increased incidence of IPA is occurring in other patient populations, such as patients with severe viral pneumonia, those on chronic steroids or other immune-suppressing therapies for autoimmune and/or rheumatological diseases, and emerging populations, such as intensive care unit patients with COVID-19 (3). Significant advancement in the prevention and treatment of IPA was noted with the development and clinical use of mold-active triazoles (voriconazole, posaconazole, and isavuconazole). However, challenges still exist. For example, resistance to triazoles has been well documented in numerous geographical locations including the United States (4–6). Additionally, patients with IPA may have complicating factors that can limit the suitability of triazole use, such as significant drug-drug interactions, prolonged QT, and pharmacokinetic (PK) variability (7). Unfortunately, traditional deoxycholate amphotericin B (AmB) and liposomal AmB (AmBisome) still have very high rates of toxicity with limited efficacy in comparison (8, 9). The development of novel antifungal drug therapy for IPA that has a different

Editor Andreas H. Groll, University Children's Hospital Münster, Germany

Address correspondence to David R. Andes, dra@medicine.wisc.edu.

D.R.A. and P.G.A. are consults of sFunga.

Received 12 December 2023
Accepted 14 January 2024
Published 6 February 2024

mechanism of action to triazoles, one that is effective and with low toxicity potential, is of substantial importance.

SF001, a next-generation polyene structurally designed to have increased specificity to the ergosterol in fungal membranes (9), demonstrates long-acting, potent, broad-spectrum fungicidal activity. SF001 is currently undergoing development. Here, we describe the use of a well-established neutropenic mouse model of IPA to characterize the PK/pharmacodynamic (PD) relationships of SF001 against *A. fumigatus* and provide a basis for the design of clinical dosing strategies.

RESULTS

In vitro susceptibility testing and *in vivo* fitness

The minimum inhibitory concentration (MIC) values of SF001, genetic mutations, and the relative fitness in the *in vivo* mouse model of each isolate are shown in Table 1. As anticipated, SF001 exhibited similar potency against wild-type (WT), *CYP51*, and *FKS1* mutant strains with similar MIC values (0.5–2.0 mg/L). The organisms also demonstrated similar *in vivo* fitness in the animal models as defined by relatively equal increases in lung organism burden in untreated mice over the study period.

Pharmacokinetics

Plasma and epithelial lining fluid (ELF) concentration-time data from the murine PK studies (Fig. 1) were used to develop a population PK model describing the PK of SF001 in mice. Candidate models were fit to the plasma and ELF data for all dose levels using the "saem" algorithm in nlmixr version 2.06 within R version 4.0.4 (10). The most robust fit to the observed data was obtained using a three-compartment model: one compartment for absorption from the intraperitoneal (IP) administration site and two compartments for systemic drug. Drug absorption was modeled using a simple absorption rate constant (ka), and elimination from plasma was linear. Interindividual variability was estimated for ka, clearance from plasma (CLt/F), volume of the central compartment (Vc/F), distributional clearance (CLd/F), and volume of the peripheral compartment (Vp/F). Residual variability was estimated using a proportional error model.

While the model that used a simple ka provided an excellent fit to the data obtained from mice administered doses of 1, 4, or 16 mg/kg (Fig. S1), the concentration-time profile observed in mice receiving the 64-mg/kg dose was substantially altered relative to the other doses such that the simple PK model did not provide an acceptable fit to the data. Fitting of a model incorporating two distinct absorption processes, one slow and one fast, to the data from the 64-mg/kg dose group alone allowed for a robust fit of all four dosing cohorts simultaneously. Distribution from plasma to ELF was modeled using simple first-order rate constants into and out of the ELF compartment and also resulted in an acceptable fit to the data (Fig. S2). The parameters for the final population PK models are provided in Table S1.

The population PK model was then used to estimate SF001 exposure in the mouse efficacy study to facilitate PK/PD analyses. This was accomplished using model-based

TABLE 1 *In vitro* activity of SF001, *in vivo* fitness in the animal model, and genetic mutations associated with drug resistance[a]

A. fumigatus isolate	SF001 dose (mg/L)	Control growth (log_{10} CE) over 96 h	Genetic profile
AF 293	1	1.40	WT
AF 41	0.5	1.93	WT
EMFR S678P	1	1.59	*FKS1* S678P (echinocandin MEC, >16 mg/L)
F11628	0.5	2.50	*CYP51* G138C
AF72	2.0	1.44	*CYP51* G54E
F14532	0.5	1.82	*CYP51* M220T

[a]CE, conidial equivalent.

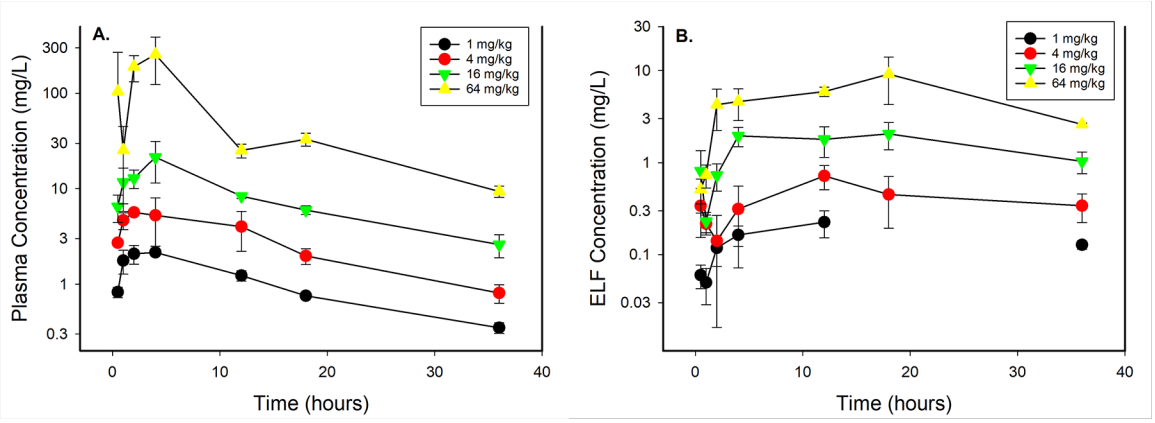

FIG 1 (A) Single-dose plasma and ELF PK of SF001. Four different doses of the SF001 that varied by fourfold concentrations on a milligram-per-kilogram basis were administered to mice by the IP route. Groups of three mice were sampled for each time point. Each symbol represents the mean ± SD for three animals. Data for the 1-mg/kg ELF 18-h time point were missing.

simulations based upon the dosage regimens used in the efficacy studies and the population means parameter estimates from the model (mrgsolve R package: Simulated from ODE-Based Population PK/PD and Systems Pharmacology Models. R package Version 0.8.6). The PK/PD indices generated for both free drug plasma and ELF included the ratio of the area under the concentration (AUC)-time curve from 0 to 24 h to the MIC (fAUC/MIC), the ratio of the free drug AUC-time curve over the 96-h study interval to the MIC ($fAUC_{0–96}$/MIC), the average fAUC/MIC for the study interval (calculated as $fAUC_{0–96}$/MIC ÷ 4), and the ratio of the free drug maximum concentrations to the MIC (fC_{max}/MIC). The free fraction assumed for the calculation of free drug in plasma was of 0.056.

Treatment efficacy and PD magnitude determination

At the start of therapy, mice had 6.86 ± 0.46 log_{10} CE/mL of lung homogenate, and the organism burden increased to 8.64 ± 0.31 log_{10} CE/mL of lung homogenate after 96 h in untreated control mice. Escalating doses of SF001 resulted in dose-dependent killing (Fig. 2). There was general congruence among the dose-response curves, which would be expected given the narrow MIC range observed *in vitro*. The two *A. fumigatus* for which the dose-response curves were shifted slightly to the right (EFMR and AF293) had the lowest SF001 MIC values. These differences are consistent with biological variability observed in this infection model. In general, at the higher SF001 doses studied, a 1- to 2-log kill was observed. The dose-response data were modeled to characterize the relationship between either the 24-h free drug AUC/MIC or C_{max}/MIC and treatment effect. Both plasma and ELF PK exposure measures were assessed in Fig. 3 and 4, respectively. A sigmoid exposure-response relationship was observed for each isolate with a strong fit for 24-h fAUC/MIC and treatment effect using plasma (R^2 0.75) and ELF (R^2 0.74) PK measures. A similarly strong relationship with the PK/PD parameter C_{max}/MIC was also demonstrated as shown in the figures. Additional PK/PD regressions [the ratio of the free drug AUC-time curve over the 96-h study interval to the MIC ($fAUC_{0–96}$/MIC), the average fAUC/MIC for the study interval (calculated as $fAUC_{0–96}$/MIC ÷ 4), and the ratio of the free drug maximum concentrations to the MIC (fC_{max}/MIC)] are shown in Fig. S3. The dose and PK/PD target exposures (24-h fAUC/MIC and C_{max}/MIC) for plasma and ELF needed to produce net stasis and 1-log_{10} reduction in organism burden for each isolate are reported in Tables 2 and 3. The median plasma 24-h fAUC/MIC ratio was 5 for a net static effect and 6.5 for 1-log_{10} kill. The median plasma C_{max}/MIC ratios for the same microbiological endpoints were 0.5 and 0.7, respectively. The median ELF 24-h AUC/MIC ratio was 13.5 for a net static effect and 15.8 for 1-log_{10} kill. The median ELF C_{max}/MIC ratios for the same microbiological endpoints were 1.1 and 1.3, respectively.

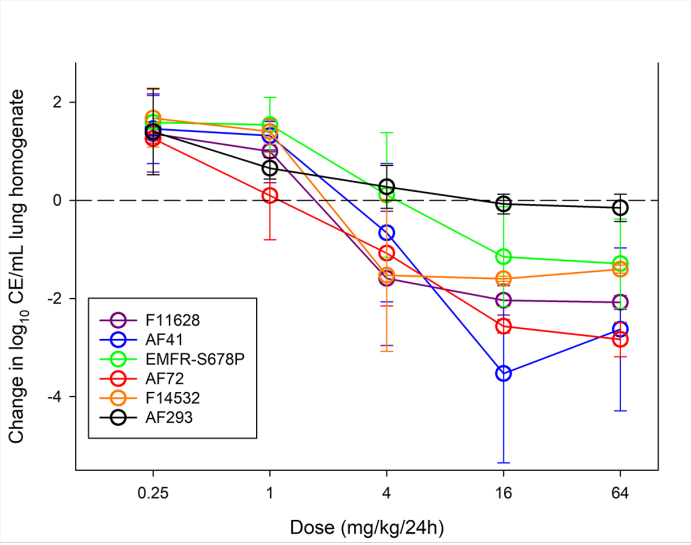

FIG 2 SF001 dose-response curves for each *A. fumigatus* isolate. Each symbol represents the mean and standard deviation from four mice. Five total drug dose levels of SF001 were given IP. Each data point is mean and standard deviation from four mice. The horizontal dashed line represents the net stasis of burden from the start of therapy. Points above the line represent an increase in burden (i.e., net growth), whereas those below the line represent a decrease in burden.

DISCUSSION

Much of the preclinical PK/PD work with polyene antifungals has been performed using *in vitro* and *in vivo* animal model studies against *Candida* spp. (11–19). These *Candida* studies have consistently demonstrated concentration-dependent activity with the PK/PD parameters C_{max}/MIC and AUC/MIC strongly associated with treatment effect (11–19). When PK/PD exposures were examined in the setting of treatment effect, a C_{max}/MIC of 2 was noted for net stasis, and maximal activity was reached at a C_{max}/MIC of approximately 10. Relatively fewer studies exist for *Aspergillus* that attempt to delineate exposure-response relationships and quantify target exposures from a PK/PD perspective. One of the earliest, an *in vitro* study against *A. fumigatus* using AmB, demonstrated a 50% effect (ED_{50}) at concentrations of approximately 0.1–0.2 mg/L, with a steep exposure-response curve with maximal effect occurring at concentrations under 1 mg/L (16). After accounting for MIC (0.25 mg/L), these concentration-effect relationships in terms of C_{max}/MIC ratio can be estimated to be approximately 0.5 and <3, respectively. Two additional *in vitro* model experiments from the same group of investigators using AmB found very congruent results with 50% inhibition of fungal growth occurring at C_{max}/MIC ratios < 0.6 and again a steep exposure-response curve with maximal effects as the value approached 1 against *A. fumigatus* (20, 21). A final *in vitro* model experiment examining AUC/MIC target exposures demonstrated an ED_{50} at AUC/MIC values of approximately 6 (19, 22). However, *in vivo* PK/PD target studies are scarce. In an *in vivo* mouse model of IPA very similar to the one reported here, the investigators demonstrated maximal survival benefit at an AmB C_{max}/MIC of 2.4 (19). Following this, an immunocompromised rabbit model study of IPA was performed, which demonstrated similar maximal antifungal efficacy at congruent C_{max}/MIC exposures (23). Taken together, the preclinical PK/PD data for AmB generally show that C_{max}/MIC ratios < 1 have been associated with antimicrobial efficacy against *A. fumigatus* and increasing C_{max}/MIC ratios to ≥1 usually lead to maximal effect.

In our current study, we demonstrate highly congruent exposure-response relationships comparable to the aforementioned studies. Notably, the exposure response was quite precipitous with small increases in C_{max}/MIC exposure leading to enhanced

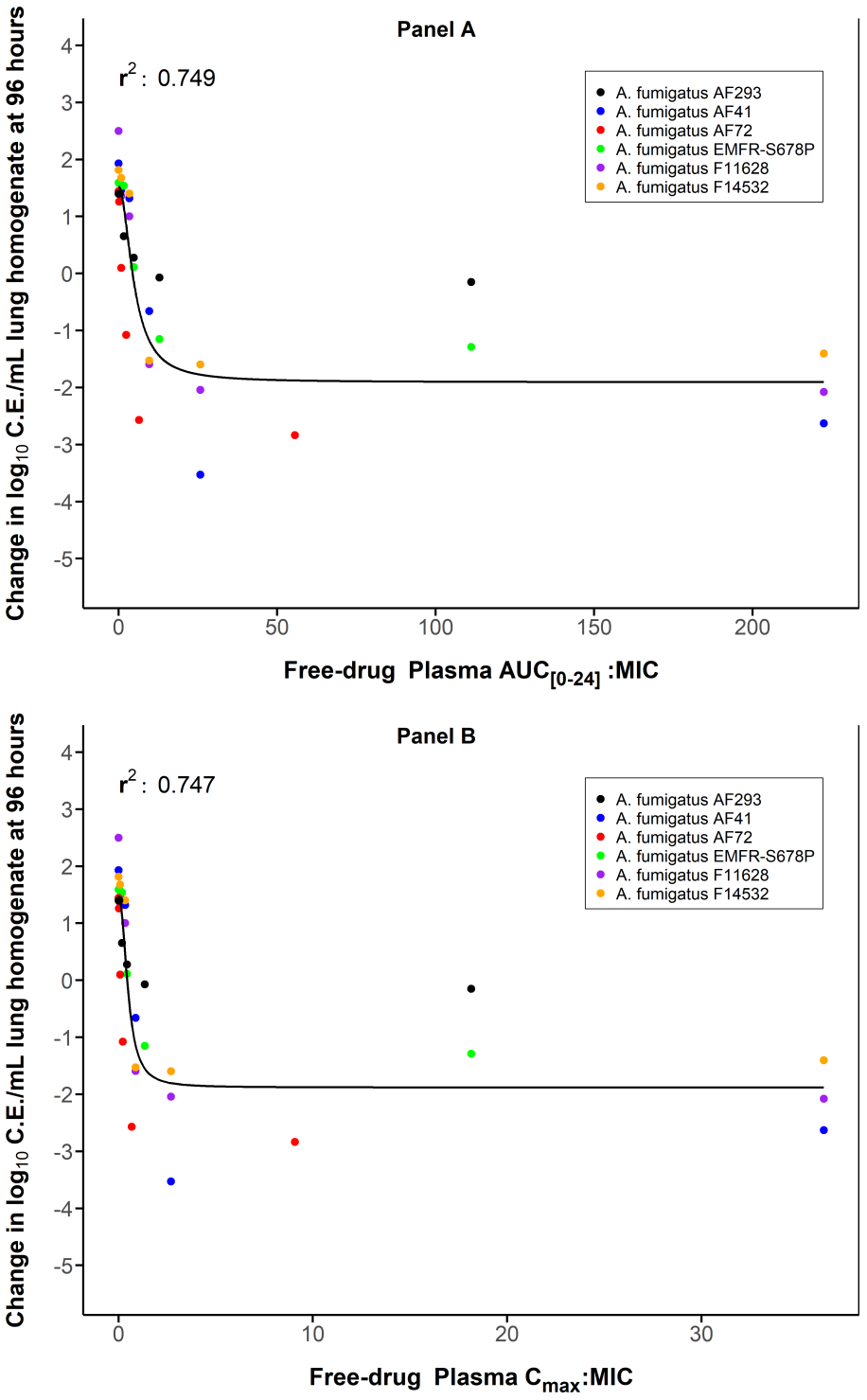

FIG 3 PD regression analysis of plasma 24-h fAUC/MIC and *in vivo* effect with SF001 against six *A. fumigatus* strains (A). PD regression analysis of plasma C_{max}/MIC and *in vivo* effect with SF001 against six *A. fumigatus* strains (B). Each symbol represents the mean from four mice. The line drawn through the data points is the best-fit line based upon the sigmoid E_{max} formula.

microbiological effect in the model. For example, in the current study, C_{max}/MIC exposures for net stasis occurred at a median value of 0.47 ± 0.28, a 1-$\log_{10}$ kill occurred at median C_{max}/MIC exposures of 0.66 ± 0.29, and the maximal effect started to plateau at C_{max}/MIC values of approximately 1. A strength of the current study is that we

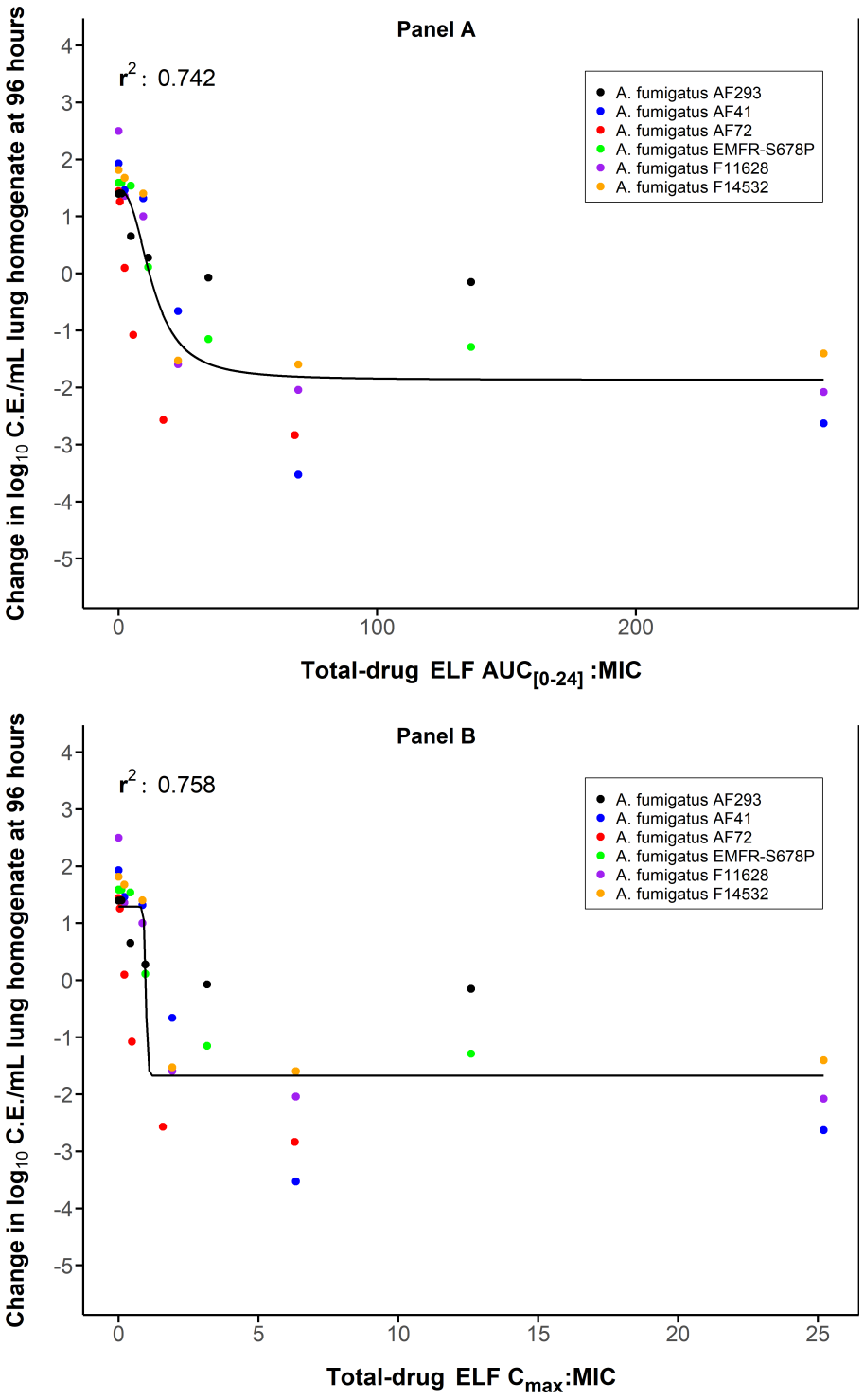

FIG 4 PD regression analysis of ELF AUC/MIC and *in vivo* effect with SF001 against six *A. fumigatus* strains (A). PD regression analysis of ELF C_{max}/MIC and *in vivo* effect with SF001 against six *A. fumigatus* strains (B). Each symbol represents the mean from four mice. The line drawn through the data points is the best-fit line based upon the sigmoid E_{max} formula.

examined both plasma and ELF exposure-response relationships, something not reported in previous studies. The exposure-response results when examined using ELF PK were similarly shaped to the plasma results, and ELF targets were numerically about twofold higher than the plasma targets. Further studies should verify this finding. It is unknown what the clinical implication of these numerically higher target exposures is

TABLE 2 SF001 plasma free drug AUC/MIC and C_{max}/MIC needed to achieve net stasis and 1-log kill endpoints for each *A. fumigatus* strain[a]

A. fumigatus isolate	MIC (mg/L)	Stasis			1-log kill		
		24-h total dose (mg/kg)	24-h plasma fAUC/MIC	Plasma C_{max}/MIC	24-h total dose (mg/kg)	24-h plasma fAUC/MIC	Plasma C_{max}/MIC
F14532	1	1.17	3.86	0.39	1.30	4.20	0.42
EMFR	0.5	4.27	5.09	0.46	9.67	9.29	0.80
AF41	1	3.87	9.43	0.78	4.07	9.83	0.93
F11628	0.5	1.59	4.92	0.48	2.80	7.16	0.66
AF72	2.0	1.33	1.02	0.10	3.25	2.00	0.19
AF293	0.5	8.90	9.51	0.87			
Mean		3.52	5.64	0.51	4.22	6.50	0.60
Median		2.73	5.01	0.47	3.25	7.16	0.66
Standard deviation		1.50	3.31	0.28	3.21	3.35	0.29

[a]1-log kill was not observed with isolate AF293.

within the ELF space. The differences in these point estimates for plasma and ELF could in part be due to the observed ELF PK variability (Fig. S2). IPA is a tissue-invasive disease; however, the organism originates in the airway and invades through ELF in order to reach tissues. Thus, ELF concentrations of antifungal may be of particular importance for prophylaxis.

Finally, it is important to note that most *Aspergillus* PK/PD studies use only one strain leading to a lack of organism variability and limited power to accurately define target exposures. The current study used six clinical strains, including WT and strains with resistance mechanisms and susceptibility to triazoles or echinocandins, and thus, the point estimates for PK/PD target exposures in the current study are likely more robust as they account for organism variability.

A limitation to the current study is the relative lack of MIC variability and/or inclusion of strains that have phenotypic resistance to AmB. This, though, is extremely common clinically, as the MIC range is usually quite narrow and resistance is exceedingly rare. Additionally, protein-binding estimates were based upon limited data from the sponsor. Further studies will be required to provide a more accurate representation of the potential concentration-dependent protein-binding characteristics of SF001.

In summary, we observed potent *in vivo* activity of SF001 that is comparable to *Aspergillus*-active triazoles previously tested in this well-established mouse model of IPA. The study demonstrates that SF001 has concentration-dependent *in vivo* efficacy against WT, azole-resistant, and echinocandin-resistant *A. fumigatus* isolates. We demonstrated that plasma C_{max}/MIC ratios approaching 1 and AUC/MIC ratios of 5–10 lead to a maximal microbiological effect in the neutropenic mouse model of IPA. The PK/PD target exposures derived in this study should be useful for designing optimized drug dosing

TABLE 3 SF001 ELF AUC/MIC and C_{max}/MIC needed to achieve net stasis and 1-log kill endpoints for each *A. fumigatus* strain

A. fumigatus isolate	MIC (mg/L)	Stasis			1-log kill		
		24-h total dose (mg/kg)	24-h ELF AUC/MIC	ELF C_{max}/MIC	24-h total dose (mg/kg)	24-h ELF AUC/MIC	ELF C_{max}/MIC
F14532	1	1.17	10.6	0.94	1.30	11.4	1
EMFR	0.5	4.27	12	0.995	9.67	20.4	1.59
AF41	1	3.87	20.4	1.66	4.07	24.3	2.05
F11628	0.5	1.59	13	1.13	2.80	17.7	1.5
AF72	2.0	1.33	2.71	0.237	3.25	5.12	0.44
AF293	0.5	8.90	22.5	1.89			
Mean		3.52	13.54	1.14	4.22	15.78	1.32
Median		2.73	12.50	1.06	3.25	17.70	1.50
Standard deviation		1.50	7.15	0.58	3.21	7.59	0.62

regimens in the clinical development of SF001 that may include front-loaded regimens to optimize the impact of C_{max} concentrations.

MATERIALS AND METHODS

Organisms, media, and antifungal

Six *A. fumigatus* isolates were chosen, including three isolates with *CYP51* mutations and one laboratory isolate with an *FKS1* mutation. Organisms were grown and subcultured on potato dextrose agar (PDA; Difco Laboratories, Detroit, MI, USA). The organisms were chosen based on similar fitness as determined by growth in the lungs of untreated animals over 96 h (Table 1). SF001 was supplied by the study sponsor (Sfunga Therapeutics). SF001 was prepared on the day of use by 5% dextrose in water containing distearoyl-rac-glycerol PEG 2000.

In vitro susceptibility testing

MICs of SF001 for the various isolates were determined using a broth microdilution method in accordance with the guidelines presented in Clinical and Laboratory Standards Institute document M38 (24). All MIC assays were performed in duplicate on three separate occasions.

Infection model

Six-week-old, specific-pathogen-free, female Institute of Cancer Research (ICR)/Swiss mice weighing 23–27 g were used for all studies (Harlan Sprague-Dawley, Indianapolis, IN, USA). Animals were maintained in accordance with the criteria of the Association for Assessment and Accreditation of Laboratory Animal Care. All animal studies were approved by the Animal Research Committee of the William S. Middleton Memorial Veterans Hospital.

A neutropenic, corticosteroid immunosuppressed mouse IPA model was utilized as previously described (25–28). Briefly, mice were rendered neutropenic (polymorph nuclear cell counts, <100/mm^3) by the subcutaneous (s.c.) injection of 150-mg/kg cyclophosphamide on Days −4 and −1 and +3 to ensure the maintenance of neutropenia until the end of study (96 h). Additionally, cortisone acetate was administered at 250 mg/kg s.c. on Day −1. Throughout the 4-day experiment, mice were also given ceftazidime at 50 mg/kg/day s.c. to prevent opportunistic bacterial infection.

Organisms were prepared by sub-culturing on PDA 5 days prior to infection and incubated at 37°C. On the day of infection, the inoculum was prepared by flooding the culture plate with 5 mL of normal saline containing 0.05% Tween 20. Gentle agitation was used to release the conidia. The conidial suspension was collected and quantified by hemocytometer (Bright-Line, Hausser Scientific, Horsham, PA, USA). The suspension was diluted in saline to a final concentration of 1×10^7 conidia/mL. Viability was confirmed by plating the suspension and performing CFU counts. Infection was produced in animals using an aspiration pneumonia model that has been successfully utilized in previous studies (26–28). Briefly, mice were anesthetized with a combination of ketamine and xylazine. Fifty microliters of the conidia suspension was pipetted into the anterior nares with mice held upright to allow aspiration into the lungs. Drug treatment commenced 2 h after the initiation of infection.

Tissue fungal burden

Pulmonary fungal burden was determined by real-time quantitative PCR (qPCR) using previously reported methods (26, 27, 29). Briefly, animals were euthanized if showing signs of distress or at the end of the 96-h experiment. Both lungs were immediately removed by aseptic technique and placed into sterile Whirl-Pak bags (Nasco, Fort Atkinson, WI, USA) containing 2 mL of sterile 0.9% normal saline. Samples were then homogenized or frozen until homogenization could occur. Homogenization of lung

tissue occurred in two steps. First, the lungs were manually homogenized using direct pressure to yield a primary homogenate. One microliter of the primary homogenate was then transferred to a sterile 2-mL screw-cap microcentrifuge tube (Sarstedt, Newton, NC, USA) with 700 µL of 425- to 600-µm acid-washed glass beads (Sigma-Aldrich, St. Louis, MO, USA). The primary homogenate was mechanically disrupted by vigorous agitation in a Bio-spec mini bead beater (Bartlesville, OK, USA) for 90 s at 4,200 rpm to yield a secondary homogenate. This secondary homogenate was stored at −20°C until DNA extraction.

DNA was extracted from secondary homogenates with the DNeasy Blood and Tissue Kit (Qiagen, Valencia, CA, USA) following the manufacturer's protocol and stored at −20°C until the day of qPCR analysis. Extracted DNA was subjected to quantitative, real-time PCR. qPCR plates were prepared on the day of the assay. Standard amounts of conidia were prepared by hemocytometer counts and were spiked into blank uninfected lungs used for generating standard curves. Samples were assayed in duplicate using a Bio-Rad CFX96 real-time system (Bio-Rad, Hercules, CA, USA). A single-copy gene, *FKS1*, was chosen for quantitation (30). Primer sequences included the following: forward primer (5′-GCCTGGTAGTGAAGCTGAGCGT-3′), reverse primer (5′-CGGTGAATGTAGGCATG TTGTCC-3′), and probe (5′-6-FAM- AGCCAGCGGCCCGCAAATG-MGB-3′) (Integrated DNA Technologies, Coralville, IA, USA). The *FKS1* mutation in strain EMFR S678P was not located in the primer-probe area of the genome and has been previously shown to not affect the quantitation reaction for that isolate (26). The primer-probe set was validated for all isolates by determining the kinetics and quantitative results for known quantities of conidia over the dynamic range (10^2 to 10^8) (26–28). The cycling conditions were as follows: activation, 50°C, 2 min; heat inactivation, 95°C, 10 min for 1 cycle; and denaturation, 95°C, 15 s; annealing and extension, 65°C, 1 min for 40 cycles. Quantitation standards were run in conjunction with each set of samples. The threshold cycle (Ct) of each sample was interpolated from a 5-point standard curve of Ct values prepared by spiking uninfected mouse lungs with known amounts of conidia (10^3 to 10^7) from each isolate being tested. Results were reported as CE per milliliter of lung homogenate.

Pharmacokinetics

Single-dose plasma and ELF PK of SF001 were performed in infected mice. Animals were administered a single IP dose (0.2 mL/dose) of SF001 at dose levels of 1, 4, 16, and 64 mg/kg. Groups of three mice were sampled at each time point (seven time points, consisting of 0.5, 1, 2, 4, 12, 18, and 36 h) and dose level. Samples were then centrifuged for 5 min at 4,000 rpm, and plasma was removed and frozen at −20°C until assay. bronchoalveolar lavage (BAL) samples were collected from mice following lavage with 1 mL of sterile saline. The recovered BAL fluid was then centrifuged to separate the alveolar macrophages (cell pellet) and the ELF (supernatant). Plasma and ELF urea concentrations were measured to allow for the calculation of ELF drug concentrations by the use of the method described by Rennard et al. (31). Urea concentrations were determined in triplicate by the use of a commercial colorimetric assay kit (Pointe Scientific, Inc.). Corrected ELF concentrations were calculated by urea correction methodology using the following formula: $[\text{Drug}]_{\text{ELF}} = [\text{Drug}]_{\text{BAL}} \times ([\text{Urea}]_{\text{plasma}}/[\text{Urea}]_{\text{BAL}})$. Total drug concentrations from ELF were utilized for all analyses. The penetration of each drug into the ELF space was calculated by comparing ELF: plasma AUC ratios. Drug assay was performed by liquid chromatography-tandem mass spectrometry (LC-MS/MS). The lower limit of detection of the LC-MS/MS assay was 0.25 mg/L.

Sample preparation

Mouse plasma analysis

Samples were prepared for LC-MS/MS analysis by protein precipitation with acetonitrile. A protein precipitation solution of 150-ng/mL AmB (*internal standard*) was prepared

in 87.5% acetonitrile. To perform protein precipitation, 25.0 µL of plasma sample was aliquoted into 200 µL of this protein precipitation solution in a labeled microcentrifuge tube. When necessary, plasma samples were diluted fourfold with blank CD-1 plasma prior to protein precipitation, such that concentrations would fall within the dynamic range of the method. Sample mixtures were vortexed vigorously for 10 min, chilled at 4°C for 25 min, and then centrifuged at 15,000 × *g* for 10 min at 4°C. Finally, 60.0 µL of each resulting supernatant was aliquoted into 300 µL of a 1:1 acetonitrile:water solution in respective wells of a 96-well plate. Following the preparation, plates were immediately placed in a 4°C auto-sampler for analysis.

Mouse BAL analysis

Samples were prepared for LC-MS/MS analysis by aliquotting 125 µL of sample into 250 µL of 20.0-ng/mL AmB (*internal standard*) in 1:1 acetonitrile:water, mixing well, and injecting 5.0 µL on column. Note that BAL samples, calibration standards, and quality control samples were stored as 1:1 sample:acetonitrile to prevent Sfu AM-2-19 from binding to tube walls. Following the preparation, plates were immediately placed in a 4°C auto-sampler for analysis.

LC-MS/MS analyses

All samples were assayed by LC-MS/MS on a Sciex 5500 with an ExionLC AC front-end. The chromatography and mass spectrometry parameters utilized for the LC-MS/MS analysis of Sfu AM-2-19 in mouse plasma and BAL fluid samples are summarized in Tables 4 and 5.

The inter-day performances of the LC-MS/MS methods utilized to quantify Sfu AM-2-19 in mouse plasma and BAL fluid are summarized in Table 6. Note that the 100* µg/mL dilution quality control samples included in the plasma analysis were diluted fourfold with blank plasma prior to preparation for LC-MS/MS analysis.

Colorimetric analysis for urea nitrogen correction

Urea nitrogen levels in mouse plasma versus BAL were utilized to correct each BAL sample for the dilution that occurs during sample collection. Mouse plasma and BAL samples were subjected to colorimetric analysis for the determination of urea nitrogen concentration using Bioassay Systems QuantiChrom Urea Assay Kit (100T) (Fisher cat# 50-107-8333).

Prior to colorimetric analysis, plasma samples were diluted 20-fold by adding 15.0 µL of sample to 285 µL of water in a microcentrifuge tube and vortexing well. Prior to colorimetric analysis, BAL samples were aliquoted (250-µL aliquots) into separate microcentrifuge tubes, dried to completion using a vacuum centrifuge, and then re-suspended in 200 µL of water. Re-suspended samples were centrifuged at 15,000 × *g* for 2 min at room temperature and then assayed directly. Select plasma and BAL samples were subjected to additional dilution for re-analysis if the initial analysis resulted in a concentration value above the dynamic range of the method.

A stock solution of 5.00-mg/dL urea was prepared using the 50-mg/dL urea stock solution from the kit above. A total of six standard solutions ranging from 0.500 to 5.00 mg/dL were prepared via serial dilution of the 5.00-mg/dL stock solution with water. Standard and unknown plasma/ELF samples were transferred into designated wells of a 96-well plate at a volume of 45.0 µL. Working reagent was prepared by mixing 1:1 Reagent A:Reagent B from the kit above. Within 20 min of working reagent preparation, 180 µL of working reagent was added to each well of the 96-well plate, and the plate was tapped lightly to mix. Following a 50-min incubation at room temperature, sample absorbance was obtained at a wavelength of 430 nm using a BioTek Synergy HT plate reader. The resulting standard curves utilized for urea nitrogen quantification were linear over 0.500–5.00 mg/dL, with R^2 values ranging from 0.9948 to 0.9975.

TABLE 4 LC-MS/MS analysis parameters

LC-MS/MS analysis of Sfu AM-2-19			
Liquid chromatography parameters		**Gradient profile**	
		Time (min)	**% B**
Column	Waters Xselect HSS T3 (50 × 2.1 mm, 3.5-µm particles)	0.00	15.0
Guard column	Waters Xselect HSS T3 (5.0 × 2.1 mm, 3.5-µm particles)	1.25	95.0
Column temperature	40°C	1.75	95.0
Mobile phase A	0.1% formic acid in H_2O	1.76	15.0
Mobile phase B	0.1% formic acid in acetonitrile	3.20	15.0
Needle wash	1:1 acetonitrile:H_2O		
Injection volume	4.00 µL (plasma); 5.00 µL (BAL)		
Total flow rate	0.5000 mL/min		
Elution	Gradient		
Total run time	3.20 min		

Plasma concentration-time data from the mouse PK studies were used to develop a population PK model describing the PK of SF001 in mice. Candidate models were fit to the plasma and ELF data for all dose levels using the "saem" algorithm in nlmixr version 2.06 within R version 4.0.4 (10). The population PK model was then used to estimate SF001 exposure in the mouse efficacy study to facilitate PK/PD analyses. This was accomplished using model-based simulations (mrgsolve R package: Simulated from ODE-Based Population PK/PD and Systems Pharmacology Models. R package Version 0.8.6) based upon the dosage regimens used in the efficacy studies and the population mean parameter estimates from the model. The PK/PD indices were generated for both free drug plasma and ELF using the model-based simulations to estimate free drug AUC/MIC, C_{max}/MIC, and time above MIC.

PK/PD index magnitude studies

Dose-response experiments using the IPA model were performed for each of the *A. fumigatus* strains. Five dose levels (consisting of 0.25, 1, 4, 16, and 64 mg/kg/day) were administered by the IP route. The treatment duration was 96 h. The dose-response relationships were quantified, and the relationship between the PK/PD index and treatment efficacy was determined using the sigmoid E_{max} model. These PK/PD relationships were examined utilizing the plasma free drug concentrations or ELF concentrations from PK studies. The coefficient of determination (R^2) from this model was used to assess the strength of this relationship. The doses required to produce a net static effect (static dose) and 1-log kill effect compared to the number of CE per milliliter of lung homogenate at the start of therapy for multiple pathogens in the IPA model were determined utilizing the plasma free drug concentrations and the following equation: $\log_{10}D = \log_{10}[E/(E_{max} - E)]/N + \log_{10} ED_{50}$, where D is the drug dose, E is the growth (as measured by qPCR and represented as CE per milliliter of lung homogenate) in untreated control mice, E_{max} is the maximal effect, N is the slope of the dose-response relationship, and ED_{50} is the dose needed to achieve 50% of the maximal effect.

TABLE 5 MS/MS analysis parameters

Mass spectrometry parameters						
Compounds	**Q1 → Q3**	**Elution time (min)**	**Declustering potential (DP)**	**Entrance potential (EP)**	**Collision energy (CE)**	**Collision Cell exit potential (CXP)**
Sfu AM-2-19	979.60 → 798.60	1.46	50.0 V	8.0 V	25.0 V	8.0 V
AmB	924.60 → 743.50	1.51	75.0 V		30.0 V	10.0 V

TABLE 6 MS/MS assay performance characteristics

LC-MS/MS method summary: AM-2-19 in mouse plasma and BAL fluid				
Matrix	**Method summary**	**Quality control**	**Inter-day % recovery**	**Inter-day %CV**
Plasma	Dynamic range: 0.250–50.000 µg/mL	0.250 µg/mL	106.5%	3.16%
		0.750 µg/mL	101.8%	5.34%
	Regression model: Linear ($1/\chi^2$)	7.50 µg/mL	104.9%	3.77%
	R^2 values: 0.9987–0.9991	35.0 µg/mL	99.0%	5.08%
		100* µg/mL	104.1%	1.58%
BAL fluid	Dynamic range: 0.0200–3.00 µg/mL	0.020 µg/mL	116.0%	2.88%
		0.070 µg/mL	105.7%	5.89%
	Regression model: Linear ($1/\chi^2$)	0.350 µg/mL	111.6%	1.59%
	R^2 values: 0.9986–0.9987	1.50 µg/mL	105.8%	1.08%

ACKNOWLEDGMENTS

This study was supported by a research grant from Sfunga Therapeutics, Inc.

AUTHOR AFFILIATIONS

[1]Department of Medicine, University of Wisconsin School of Medicine and Public Health, Madison, Wisconsin, USA
[2]Institute for Clinical Pharmacodynamics, Schenectady, New York, USA
[3]Department of Medical Microbiology and Immunology, University of Wisconsin, Madison, Wisconsin, USA
[4]William S. Middleton Memorial VA Hospital, Madison, Wisconsin, USA

AUTHOR ORCIDs

Brian VanScoy http://orcid.org/0000-0001-6527-1475
Chris Rubino http://orcid.org/0000-0003-3172-0847
Paul G. Ambrose http://orcid.org/0000-0002-2230-1125
David R. Andes http://orcid.org/0000-0002-7927-9950

AUTHOR CONTRIBUTIONS

Alexander J. Lepak, Formal analysis, Writing – original draft | Brian VanScoy, Methodology, Writing – review and editing | Paul G. Ambrose, Writing – original draft, Writing – review and editing | David R. Andes, Conceptualization, Formal analysis, Funding acquisition, Investigation, Methodology, Supervision, Writing – original draft, Writing – review and editing.

ADDITIONAL FILES

The following material is available online.

Supplemental Material

Supplemental table and figures (AAC01631-23-S0001.pdf). Fig. S1 and S2 and Table S1.

REFERENCES

1. Patterson TF, Thompson GR, Denning DW, Fishman JA, Hadley S, Herbrecht R, Kontoyiannis DP, Marr KA, Morrison VA, Nguyen MH, Segal BH, Steinbach WJ, Stevens DA, Walsh TJ, Wingard JR, Young J-A, Bennett JE. 2016. Practice guidelines for the diagnosis and management of aspergillosis: 2016 update by the infectious diseases society of America. Clin Infect Dis 63:e1–e60. https://doi.org/10.1093/cid/ciw326
2. Ullmann AJ, Aguado JM, Arikan-Akdagli S, Denning DW, Groll AH, Lagrou K, Lass-Flörl C, Lewis RE, Munoz P, Verweij PE, et al. 2018. Diagnosis and management of *Aspergillus* diseases: executive summary of the 2017 ESCMID-ECMM-ERS guideline. Clin Microbiol Infect 24:e1–e38. https://doi.org/10.1016/j.cmi.2018.01.002
3. Cadena J, Thompson GR 3rd, Patterson TF. 2016. Invasive aspergillosis: current strategies for diagnosis and management. Infect Dis Clin North Am 30:125–142. https://doi.org/10.1016/j.idc.2015.10.015

4. Wiederhold NP, Patterson TF. 2015. Emergence of azole resistance in *Aspergillus*. Semin Respir Crit Care Med 36:673–680. https://doi.org/10.1055/s-0035-1562894
5. Lestrade PPA, Meis JF, Melchers WJG, Verweij PE. 2019. Triazole resistance in *Aspergillus fumigatus*: recent insights and challenges for patient management. Clin Microbiol Infect 25:799–806. https://doi.org/10.1016/j.cmi.2018.11.027
6. Etienne KA, Berkow EL, Gade L, Nunnally N, Lockhart SR, Beer K, Jordan IK, Rishishwar L, Litvintseva AP, Cowen LE. 2021. Genomic diversity of azole-resistant *Aspergillus fumigatus* in the United States. mBio 12:e0180321. https://doi.org/10.1128/mBio.01803-21
7. Echeverria-Esnal D, Martín-Ontiyuelo C, Navarrete-Rouco ME, Barcelo-Vidal J, Conde-Estévez D, Carballo N, De-Antonio Cuscó M, Ferrández O, Horcajada JP, Grau S. 2022. Pharmacological management of antifungal agents in pulmonary aspergillosis: an updated review. Expert Rev Anti Infect Ther 20:179–197. https://doi.org/10.1080/14787210.2021.1962292
8. Herbrecht R, Kuessner D, Pooley N, Posthumus J, Escrig C. 2018. Systematic review and network meta-analysis of clinical outcomes associated with isavuconazole versus relevant comparators for patients with invasive aspergillosis. Curr Med Res Opin 34:2187–2195. https://doi.org/10.1080/03007995.2018.1502659
9. Yang YL, Xiang ZJ, Yang JH, Wang WJ, Xu ZC, Xiang RL. 2021. Adverse effects associated with currently commonly used antifungal agents: a network meta-analysis and systematic review. Front Pharmacol 12:697330. https://doi.org/10.3389/fphar.2021.697330
10. Fidler M, Wilkins JJ, Hooijmaijers R, Post TM, Schoemaker R, Trame MN, Xiong Y, Wang W. 2019. Nonlinear mixed-effects model development and simulation using nlmixr and related R open-source packages. CPT Pharmacometrics Syst Pharmacol 8:621–633. https://doi.org/10.1002/psp4.12445
11. Andes D, Safdar N, Marchillo K, Conklin R. 2006. Pharmacokinetic-pharmacodynamic comparison of amphotericin B (AMB) and two lipid-associated AMB preparations, liposomal AMB and AMB lipid complex, in murine candidiasis models. Antimicrob Agents Chemother 50:674–684. https://doi.org/10.1128/AAC.50.2.674-684.2006
12. Andes D, Stamsted T, Conklin R. 2001. Pharmacodynamics of amphotericin B in a neutropenic-mouse disseminated-candidiasis model. Antimicrob Agents Chemother 45:922–926. https://doi.org/10.1128/AAC.45.3.922-926.2001
13. Ernst EJ, Klepser ME, Pfaller MA. 2000. Postantifungal effects of echinocandin, azole, and polyene antifungal agents against *Candida albicans* and *Cryptococcus neoformans*. Antimicrob Agents Chemother 44:1108–1111. https://doi.org/10.1128/AAC.44.4.1108-1111.2000
14. Groll AH, Lyman CA, Petraitis V, Petraitiene R, Armstrong D, Mickiene D, Alfaro RM, Schaufele RL, Sein T, Bacher J, Walsh TJ. 2006. Compartmentalized intrapulmonary pharmacokinetics of amphotericin B and its lipid formulations. Antimicrob Agents Chemother 50:3418–3423. https://doi.org/10.1128/AAC.00241-06
15. Klepser ME, Wolfe EJ, Jones RN, Nightingale CH, Pfaller MA. 1997. Antifungal pharmacodynamic characteristics of fluconazole and amphotericin B tested against candida albicans. Antimicrob Agents Chemother 41:1392–1395. https://doi.org/10.1128/AAC.41.6.1392
16. Lewis RE, Wiederhold NP, Klepser ME. 2005. *In vitro* pharmacodynamics of amphotericin B, itraconazole, and voriconazole against *Aspergillus*, *Fusarium*, and *Scedosporium* spp. Antimicrob Agents Chemother 49:945–951. https://doi.org/10.1128/AAC.49.3.945-951.2005
17. Seyedmousavi S, Melchers WJG, Mouton JW, Verweij PE. 2013. Pharmacodynamics and dose-response relationships of liposomal amphotericin B against different azole-resistant *Aspergillus fumigatus* isolates in a murine model of disseminated aspergillosis. Antimicrob Agents Chemother 57:1866–1871. https://doi.org/10.1128/AAC.02226-12
18. Warn PA, Morrissey J, Moore CB, Denning DW. 2000. *In vivo* activity of amphotericin B lipid complex in immunocompromised mice against fluconazole-resistant or fluconazole-susceptible *Candida tropicalis*. Antimicrob Agents Chemother 44:2664–2671. https://doi.org/10.1128/AAC.44.10.2664-2671.2000
19. Wiederhold NP, Tam VH, Chi J, Prince RA, Kontoyiannis DP, Lewis RE. 2006. Pharmacodynamic activity of amphotericin B deoxycholate is associated with peak plasma concentrations in a neutropenic murine model of invasive pulmonary aspergillosis. Antimicrob Agents Chemother 50:469–473. https://doi.org/10.1128/AAC.50.2.469-473.2006
20. Elefanti A, Mouton JW, Verweij PE, Zerva L, Meletiadis J. 2014. Susceptibility breakpoints for amphotericin B and *Aspergillus* species in an *in vitro* pharmacokinetic-pharmacodynamic model simulating free-drug concentrations in human serum. Antimicrob Agents Chemother 58:2356–2362. https://doi.org/10.1128/AAC.02661-13
21. Al-Saigh R, Siopi M, Siafakas N, Velegraki A, Zerva L, Meletiadis J. 2013. Single-dose pharmacodynamics of amphotericin B against *Aspergillus* species in an *in vitro* pharmacokinetic/pharmacodynamic model. Antimicrob Agents Chemother 57:3713–3718. https://doi.org/10.1128/AAC.02484-12
22. Lestner JM, Howard SJ, Goodwin J, Gregson L, Majithiya J, Walsh TJ, Jensen GM, Hope WW. 2010. Pharmacokinetics and pharmacodynamics of amphotericin B deoxycholate, liposomal amphotericin B, and amphotericin B lipid complex in an *in vitro* model of invasive pulmonary aspergillosis. Antimicrob Agents Chemother 54:3432–3441. https://doi.org/10.1128/AAC.01586-09
23. Al-Nakeeb Z, Petraitis V, Goodwin J, Petraitiene R, Walsh TJ, Hope WW. 2015. Pharmacodynamics of amphotericin B deoxycholate, amphotericin B lipid complex, and liposomal amphotericin B against *Aspergillus fumigatus*. Antimicrob Agents Chemother 59:2735–2745. https://doi.org/10.1128/AAC.04723-14
24. Reference method for broth dilution antifungal susceptibility testing of filamentous fungi, M38. 2017. In Institute CLS
25. Zhao M, Lepak AJ, Marchillo K, Vanhecker J, Sanchez H, Ambrose PG, Andes DR. 2019. APX001 pharmacokinetic/pharmacodynamic target determination against *Aspergillus fumigatus* in an *in vivo* model of invasive pulmonary aspergillosis. Antimicrob Agents Chemother 63:e02372-18. https://doi.org/10.1128/AAC.02372-18
26. Lepak AJ, Marchillo K, Vanhecker J, Andes DR. 2013. Posaconazole pharmacodynamic target determination against wild-type and cyp51 mutant isolates of *Aspergillus fumigatus* in an *in vivo* model of invasive pulmonary aspergillosis. Antimicrob Agents Chemother 57:579–585. https://doi.org/10.1128/AAC.01279-12
27. Lepak AJ, Marchillo K, VanHecker J, Andes DR. 2013. Impact of *in vivo* triazole and echinocandin combination therapy for invasive pulmonary aspergillosis: enhanced efficacy against cyp51 mutant isolates. Antimicrob Agents Chemother 57:5438–5447. https://doi.org/10.1128/AAC.00833-13
28. Lepak AJ, MarchilloK, Vanhecker J, Andes DR. 2013. Isavuconazole (BAL4815) pharmacodynamic target determination in an *in vivo* murine model of invasive pulmonary aspergillosis against wild-type and cyp51 mutant isolates of *Aspergillus fumigatus*. Antimicrob Agents Chemother 57:6284–6289. https://doi.org/10.1128/AAC.01355-13
29. Bowman JC, Abruzzo GK, Anderson JW, Flattery AM, Gill CJ, Pikounis VB, Schmatz DM, Liberator PA, Douglas CM. 2001. Quantitative PCR assay to measure *Aspergillus fumigatus* burden in a murine model of disseminated aspergillosis: demonstration of efficacy of caspofungin acetate. Antimicrob Agents Chemother 45:3474–3481. https://doi.org/10.1128/AAC.45.12.3474-3481.2001
30. Herrera ML, Vallor AC, Gelfond JA, Patterson TF, Wickes BL. 2009. Strain-dependent variation in 18S ribosomal DNA copy numbers in *Aspergillus fumigatus*. J Clin Microbiol 47:1325–1332. https://doi.org/10.1128/JCM.02073-08
31. Rennard SI, Basset G, Lecossier D, O'Donnell KM, Pinkston P, Martin PG, Crystal RG. 1986. Estimation of volume of epithelial lining fluid recovered by lavage using urea as marker of dilution. J Appl Physiol (1985) 60:532–538. https://doi.org/10.1152/jappl.1986.60.2.532